

Doping effect on thermoelectric properties of MoS₂

HUAIHONG GUO¹, TENG YANG¹ ^(a), PENG TAO¹ and ZHIDONG ZHANG¹

¹ *Shenyang National Laboratory for Materials Science, Institute of Metal Research and International Centre for Materials Physics, Chinese Academy of Sciences, 72 Wenhua Road, Shenyang 110016, PRC*

PACS 72.20.Pa – Thermoelectric and thermomagnetic effects

PACS 72.80.Ga – Transition-metal compounds

PACS 31.15.A- – Ab initio calculations

Abstract –We systematically study thermoelectric properties of layered MoS₂ by doping, based on Boltzmann transport theory and first-principles calculations. We obtain optimal doping region (around 10^{19} cm⁻³) by looking closely to the temperature and doping level dependent thermopower, electrical conductivity, power factor (PF) and ultimately figure of merit (ZT) coefficient along in-plane and cross-plane directions. MoS₂ has a vanishingly small anisotropy of thermopower but a big anisotropy of electrical conductivity and electronic thermal conductivity in optimal doping region. κ_e is comparable to κ_l in the plane while κ_l dominates over κ_e across the plane. ZT can reach as high as 0.3 at around 700 K. In-plane direction is demonstrated to be more preferable for thermoelectric applications of MoS₂ by doping.

Introduction. – Thermoelectrics play a key role for power generation and refrigeration [1–3]. Chalcogenide composite materials, such as Bi₂Te₃, PbTe and others [4–10], have attracted much research interest for decades because of their high performance on thermoelectric conversion. Transition-metal dichalcogenide MoS₂, one prototype material in chalcogenide family, has distinctive electronic, mechanical, catalytic and tribological properties [11–20]. Recent research on its optical properties [21] and lattice dynamics [22, 23] has aroused renewed interest but its thermoelectric properties have barely been studied [24]. Nevertheless, the lowest thermal conductivity obtained experimentally in a MoS₂-related structure [25], together with an unusually large thermopower [26–28] found in MoS₂, may render it a promising candidate for thermoelectric application.

Unfortunately, available experimental data concerning the thermoelectric transport properties of MoS₂ are quite scarce and fragmentary in literature. The most significant experimental work was performed by Mansfield and Salam [27] and Thakurta et. al. [26], who studied temperature dependence of the electrical transport properties including thermopower and electrical conductivity at only three samples with low dopings, but failed to investigate on the thermal-related properties. Kim et. al. [29] merely worked on the thermal conductivity κ . Based on these

incomplete experimental data, it is difficult to estimate the figure of merit ZT coefficient which is crucial to evaluate thermoelectric conversion capability. Moreover, available extrinsic carrier concentrations in MoS₂ single crystals were quite low. It remains a big challenge to obtain a wide doping region in experiment but nonetheless is essential to tuning carrier density appropriate for an optimum ZT.

In this letter, we study theoretically the thermoelectric transport properties of MoS₂ over a range of doping level (from 10^{15} to 10^{20} cm⁻³) for an optimization of its thermoelectric conversion efficiency. We have the following findings: (1) Thermopower is attainable more than 200 μ V/K over a wide range of dopings and directional anisotropy vanishes between in-plane and cross-plane thermopowers for doping level above 10^{17} cm⁻³. (2) Anisotropic electronic scattering time exists between in-plane and cross-plane directions, which accounts for two orders of magnitude difference between electrical conductivities σ_{xx} and σ_{zz} and also gives rise to anisotropy between electronic thermal conductivity κ_e^{xx} and κ_e^{zz} . (3) In optimal doping region, κ_e is comparable to κ_l in the plane while κ_l dominates over κ_e across the plane. (4) Carrier density around 10^{19} cm⁻³ is sufficient for optimal thermoelectric performance, figure of merit ZT coefficient reaches 0.3 at 700K within the plane. (5) A preference for in-plane over cross-plane direction by doping for thermoelectric applications of MoS₂ is demonstrated.

^(a) E-mail: yangteng@imr.ac.cn

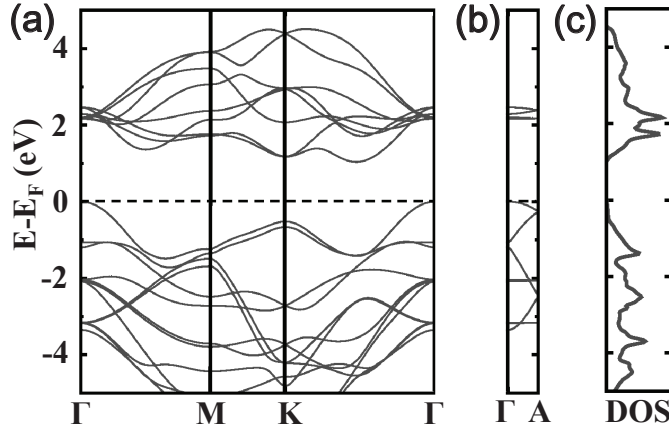


Fig. 1: (Color online) EV-GGA electronic band structure of MoS₂ along high-symmetry lines (a) Γ -M-K- Γ in plane and (b) Γ -A across plane in the hexagonal Brillouin zone (BZ). The valence-band edge is set as zero and marked with a dashed line. Electronic density of states in (c) shows a comparatively higher value at the conduction band edge than at the valence band edge.

METHODOLOGY. — The band structure of MoS₂ is calculated by using the general potential linearized augmented plane-wave(LAPW) method as implemented in the WIEN2K package [30]. The electronic exchange-correlation is described within the generalized gradient approximation (GGA) of Perdew-Burke-Ernzerhof(PBE) flavor [31]. We use 5000 k points in the full Brillouin zone(BZ) to achieve a total energy convergence better than 1 meV/atom. MoS₂ has P_{63}/mmc space group symmetry and consists of a hexagonal plane of molybdenum atoms sandwiched by two hexagonal planes of sulfur atoms. The unit cell contains two alternating and weakly van-der-Waals-bonded layers with an AB stacking along c axis. The experimental lattice parameters [32] ($a = 3.16\text{\AA}$, $c = 12.295\text{\AA}$) are used here.

We calculate transport properties based on Boltzmann transport theory applied to the band structure. In the following part, we discuss the dependence of transport functions including thermopower S , electrical conductivity σ , power factor(PF), and ultimately figure of merit coefficient ZT on temperature and doping level along two perpendicular directions. The electron scattering time is assumed to be independent of energy due to its good description of $S(T)$ in a number of thermoelectric materials [6, 33, 34]. In this sense, no adjustable parameters are needed to calculate those transport functions. The integration is done within the BOLTZTRAP transport code [35]. A very dense mesh with up to 18000 k points in the BZ is used.

RESULTS AND DISCUSSION. — An improved band gap is essential for calculating transport properties, so the Engel-Vosko GGA (EV-GGA) formalism [36] is applied to calculate the band gap more accurately. In Fig. 1, we present our calculated band structure and density of

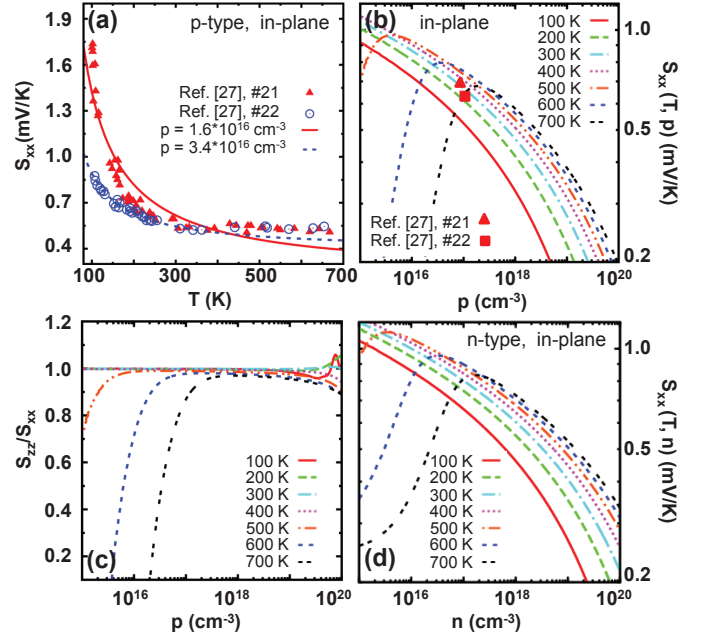


Fig. 2: (Color online) (a) Temperature dependence of calculated in-plane thermopower S_{xx} of MoS₂, compared with experimental data by Mansfield and Salam [27] at two doping levels $p = 1.6 \times 10^{16}$ (filled triangle) and 3.4×10^{16} (empty circle) holes per cm^3 . Doping level dependence of (b) in-plane thermopower $S_{xx}(p, T)$, (c) ratio of cross-plane $S_{zz}(p, T)$ over in-plane $S_{xx}(p, T)$ and (d) in-plane $S_{xx}(n, T)$ at different temperatures. The temperature ranges from 100K to 700K for some practical reason. Hole and electron doping are respectively used in (a-c) and (d). Experimental data with $p = 7.6 \times 10^{16}$ and $1.0 \times 10^{17} \text{ cm}^{-3}$ at 200K by Mansfield and Salam [27] is respectively marked by filled triangle and square in (b).

states of MoS₂. The in-plane and cross-plane cases are considered separately in Fig. 1(a, b). In Fig. 1(a), an indirect gap of 1.04 eV is obtained between top of valence band at Γ and bottom of conduction band at one k point from K to Γ . A similar band structure calculated from standard PBE-GGA formalism gives an indirect gap of 0.84 eV, which agrees with reported value [37]. Compared with $\Delta_i \sim 1.20 \text{ eV}$ from experiment [38], it is clear that EV-GGA does improve the band gap calculation upon PBE-GGA. In contrast to the pronounced dispersive in-plane electronic bands shown in Fig. 1(a), the cross-plane bands shown in Fig. 1(b) are quite flat, showing a very weak cross-plane bonding due to Van der Waals interaction. The structural anisotropy induces an anisotropy between in-plane and cross-plane band gaps. The calculated cross-plane gap is found to be 2.20 eV.

Besides the band gap anisotropy, a strong asymmetric feature of band structure between valence and conduction bands implies that the thermoelectric properties of n-type MoS₂ would be very different from that of p-type. The heavy and doubly degenerate bands near the conduction-band minimum suggest that the n-type MoS₂ would have

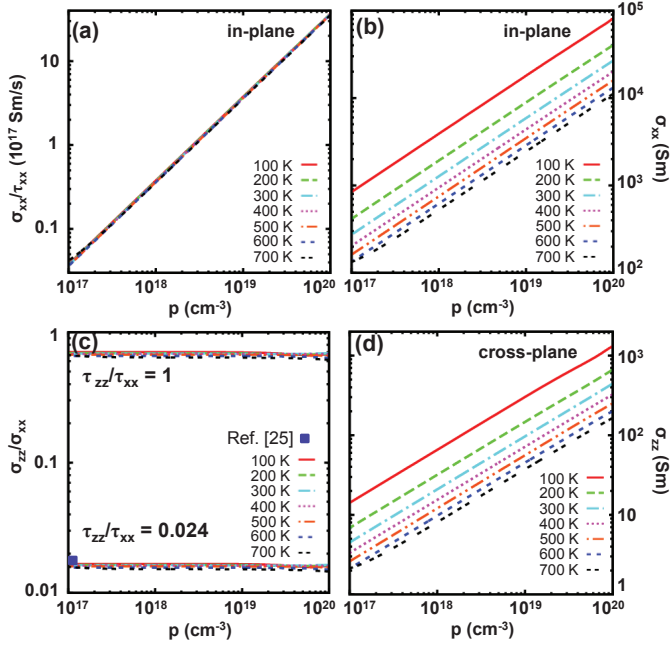


Fig. 3: (Color online) Doping level dependence of (a) in-plane σ_{xx}/τ_{xx} , (b) in-plane electrical conductivity σ_{xx} , (c) ratio of cross-plane σ_{zz}/τ_{zz} over in-plane σ_{xx}/τ_{xx} and (d) cross-plane σ_{zz} , at different temperatures. Isotropic and anisotropic electronic scattering time τ are respectively assumed in (c), for instance, $\tau_{zz}/\tau_{xx} = 1$ and 0.024 with the anisotropic one fitting well the experimental data in blue square from Thakurta et. al. [26] and thereby used to derive σ_{zz} in (d).

better thermoelectric performance. In Fig. 1(c), total density of states (DOS) also shows this preference, there is a comparatively higher DOS very close to the conduction band edge than that near the valence band edge. Considering more experimental data are found for p-type in literature [26–28], we focus on hole-doped MoS₂ in this study.

In-plane and cross-plane thermopower are firstly studied. We initially compare our calculated S with experimental data from Mansfield and Salam [27] in Fig. 2(a,b). Samples in their experiment were p-type from nature with hole carrier concentration as low as $10^{15} \sim 10^{17}$ cm⁻³. A very good agreement is obtained. Both our calculation and available experimental data show a value of in-plane thermopower S higher than $400 \mu V/K$ and S decreases with increasing temperature as shown in Fig. 2(a). Then we extend our discussion to high doping of $10^{17} \sim 10^{20}$ cm⁻³ (corresponding to $p = 10^{-5} \sim 10^{-2}$ holes per unit cell in our case) where thermoelectric properties are expected to be optimized as predicted from theory [39] and experimentally observed in many materials [40–42]. It also applies in MoS₂ as we will show later. From Fig. 2(b), the thermopower in the high doping region, though decreasing with doping level, takes a value of at least $200 \mu V/K$ ($ZT > 2.4$ is expected from the Wiedemann-Franz law.) and increases with increasing temperature. To see

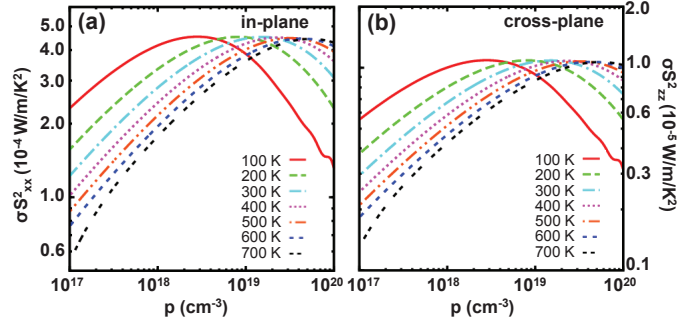


Fig. 4: (Color online) Doping level dependence of (a) power factor $\sigma_{xx} S_{xx}^2$ and (b) $\sigma_{zz} S_{zz}^2$ of p-type MoS₂ at different temperatures.

a possible anisotropy between in-plane and cross-plane S , we then show the ratio of S_{zz} over S_{xx} in Fig. 2(c). A relatively high anisotropy of thermopower below 10^{17} cm⁻³, possibly due to difference of effective mass (or mobility) and density between band-edge carriers moving along two directions, according to the Mott formula [43] $S \sim \frac{\partial \ln(n\mu)}{\partial E}$ where n , μ are respectively carrier density and mobility. Anisotropy vanishes as doping goes above 10^{17} cm⁻³ and both S_{xx} and S_{zz} show similar magnitude and dependence on hole doping level and temperature, which is different from layered conductive thermoelectric oxides [44,45]. Finally, to confirm that n-type MoS₂ may be better, we briefly compare n-type in Fig. 2(d) with p-type in Fig. 2(b). Expectedly, bigger value of thermopower of n-type MoS₂ than of p-type is found.

Based on the energy-independent scattering time approximation, it is quite straightforward to get doping dependence of σ/τ at various temperature from the electronic band structure, upon which we calculate σ if τ is known. In Fig. 3(a), we show calculated σ_{xx}/τ_{xx} depending on hole doping and temperature. We find an almost temperature independence but an approximately linear doping level dependence of σ_{xx}/τ_{xx} , namely $\sigma_{xx}/\tau_{xx} \sim T^0 p$. For a quadratic band dispersion in an electron-phonon approximation, $\sigma \sim p^{\frac{2}{3}} T^{-1}$ stands, this results in $\tau_{xx} \sim T^{-1} p^{-\frac{1}{3}}$, in consistent with the analytical treatment of carriers scattered by lattice vibrations in a semiconductor [6,43]. To calculate σ_{xx} , we need some experimental input to get $\tau_{xx}(T, p)$. Here we use $\sigma_{xx} = 0.16 \Omega^{-1} cm^{-1}$ at 100 K and 1.4×10^{15} cm⁻³ doping level from the experimental data by Thakurta et. al. [26] and get $\tau_{xx} = 3.04 \times 10^{-6} T^{-1} p^{-\frac{1}{3}}$ with Kelvin and cm⁻³ as the unit of T and p , respectively. Plugging it into our calculated σ/τ , we show $\sigma_{xx}(T, p)$ in Fig. 3(b), and power factor $\sigma_{xx} S_{xx}^2(T, p)$ in Fig. 4(a).

Electrical conductivity along c axis is also calculated and a strong anisotropy is found between the in-plane and cross-plane carrier scattering time τ . When isotropic τ is assumed, namely, $\tau_{zz}/\tau_{xx} = 1$, we obtain σ_{zz}/σ_{xx} close to unity in Fig. 3(c), which is against the reported result [26]. To fit σ_{xx}/σ_{zz} of two orders of magnitude in experiment,

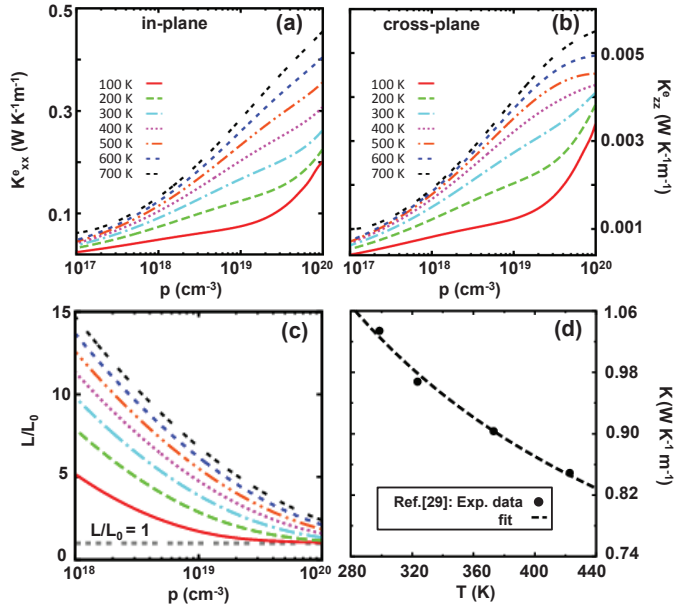


Fig. 5: (Color online) (a) In-plane electronic thermal conductivity κ_{xx}^e , (b) cross-plane κ_{zz}^e and (c) in-plane L/L_0 as function of doping and temperature. $L = \kappa/(\sigma T)$ and L_0 is the Lorenz number $2.44 \times 10^{-8} \text{ W}\Omega\text{K}^{-2}$. (d) Temperature dependence of thermal conductivity κ from experiment by Kim et. al. [29], which are presented by filled circles and fitted by $\kappa = 183.103/T + 0.412671$ in dashed line.

we use anisotropic $\tau_{zz}/\tau_{xx} = 0.024$, which suggests that a strong anisotropy of carrier scattering time should play a role in this system, and therefore obtain $\tau_{zz} = 7.30 \times 10^{-8} \text{ T}^{-1} \text{ p}^{-\frac{1}{3}}$. Finally, we are able to calculate $\sigma_{zz}(T, p)$ and show it in Fig. 3(d).

With thermopower and electrical conductivity available, we are able to evaluate power factor. For an optimized thermoelectric performance, peak value of PF, the corresponding doping level and temperature are more concerned here. Both power factors along two perpendicular directions have peak values spanning in a wide doping range from 10^{17} to 10^{20} cm^{-3} . From Fig. 4, the value of peak power factor is nearly constant, while its temperature increases with the hole doping level. Due to the anisotropic carrier scattering time τ , nearly 50-fold difference is found between in-plane and cross-plane power factors, e.g., σS_{xx}^2 and σS_{zz}^2 maxima at 700 K are respectively $4.1 \times 10^{-4} \text{ W/m/K}^2$ and $1.0 \times 10^{-5} \text{ W/m/K}^2$. The in-plane PF value is close to that of good thermoelectric materials [39].

To optimize ZT value, it is also essential to know thermal conductivity κ , including electronic κ_e and lattice κ_l . Based on the scattering time approximation previously discussed, we firstly calculate electronic thermal conductivity and show it in Fig. 5(a,b). κ_e increases with carrier density p and temperature. At least two orders of magnitude difference between κ_{xx}^e and κ_{zz}^e are found, which is consistent with electrical conductivity case. Usually

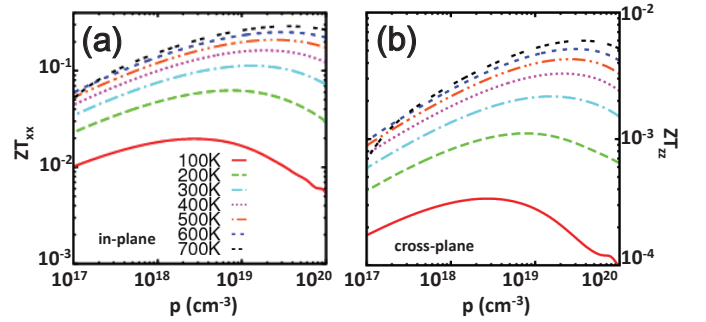


Fig. 6: (Color online) Doping level dependent (a) in-plane and (b) cross-plane figure of merit coefficient ZT of p-type MoS₂ at different temperatures. The experimental thermal conductivities κ from Fig.5(d) were used.

one gets κ_e from electrical conductivity σ by using the Wiedemann-Franz law, namely $\kappa_e/(\sigma T) = 2.44 \times 10^{-8} \text{ W}\Omega\text{K}^{-2}$, the so-called Lorenz number. However, it seems not the case here. In Fig.5(c) we normalize $L(=\kappa_e/(\sigma T))$ by the Lorenz number and plot it as function of doping and temperature. L/L_0 is close to one as carrier density goes beyond 10^{20} cm^{-3} . Unlike the electronic κ_e , the lattice κ_l can't be calculated from electronic band structure. Here we simply use experimental data from literature [29] and show it in Fig. 5(d). Kim et. al. [29] measured temperature dependence of κ for MoS₂ sample as shown by filled circles in Fig.5(d). The lattice thermal conductivity dominates in the cross-plane direction, with two orders of magnitude bigger than κ_{zz}^e . While the in-plane κ_l is comparable to κ_e . We fit the experimental data by using $\kappa = 183.103/T + 0.412671$. It seems that Umklapp process which usually has $\kappa \sim 1/T$ shows up and thermal conductivity gets softening with increasing temperature.

All the data obtained above allow us to calculate ZT as function of temperature and hole doping along two directions, which is shown in Fig. 6(a-d). Optimum ZT value increases with increasing temperature, so does the corresponding optimum doping level. In-plane is better than cross-plane for thermoelectric conversion, with its ZT up to 0.30 and saturated around 700 K, as shown in Fig.6(a,b). We may further reduce κ by random stacking according to Kim [29] and Chiritescu et. al. [25], but its effect on electrical transport needs to be checked if it may compromise the gain of ZT by reducing thermal conductivity.

CONCLUSION. – By combining ab. initio. band structure calculation with semi-classical Boltzmann transport theory, we theoretically studied the doping and temperature dependence of thermoelectric transport properties of 2H-MoS₂. Anisotropic electronic scattering time has to be considered to account for difference between in-plane and cross-plane electrical conductivity σ , which also gives rise to anisotropy of electronic thermal conductivity κ_e . In-plane κ_{xx}^e is comparable to lattice κ_l^{xx} while cross-plane lattice κ_l^{zz} dominates over lattice κ_e^{zz} . In contrast to

the anisotropy of σ and κ_e , thermopower, which is attainable more than $200 \mu\text{V/K}$ over a wider range of doping and temperature, shows a vanishing anisotropy for doping over 10^{17} cm^{-3} . The maximum ZT can reach as high as 0.3 at around 700 K with carrier density of 10^{20} cm^{-3} , and may go higher if restacking process is used to further reduce the thermal conductivity. A preference for the in-plane thermoelectric transport by doping is demonstrated.

* * *

This work was supported by the NSFC under Grant No. 11004201, 50831006 and the National Basic Research Program (No. 2012CB933103). T.Y. acknowledges the IMR SYN-Young Merit Scholars and T.S. Kê research grant for support.

REFERENCES

- [1] Brian C. Sales, Science **295**, 1248 (2002).
- [2] A. Majumdar, Science **303**, 777(2004).
- [3] H. Böttner et. al., MRS Bull. **31**, 211 (2006).
- [4] T. Tritt (Vol. Editor), *Recent Trends in Thermoelectric Materials Research* vol. **69-71** (Semiconductors & Semimetals) Academic Press, San Diego (2001).
- [5] J. Androulakis et. al., Phys. Rev. B **83**, 195209 (2011).
- [6] K.P. Ong, D.J. Singh and P. Wu, Phys. Rev. B **83**, 115110 (2011).
- [7] D. Parker and D.J. Singh, Phys. Rev. B **82**, 035204 (2010).
- [8] H. Goldsmid, A. Sheard, D. Wright, Br. J. Appl. Phys. **9**, 365 (1958).
- [9] R. Venkatasubramanian, E. Siivola, T. Colpitts, Nature **413**, 597 (2001).
- [10] N. F. Hinsche, B. Yu. Yavorsky, I. mertig, P. Zahn, Phys. Rev. B **84**, 165214 (2011).
- [11] L. Rapoport et. al., Nature(London) **387**, 791 (1997).
- [12] J.M. Martin et. al., Phys. Rev. B **48**, 10583–10586 (1993).
- [13] B.C. Gates, Catalytic Chemistry, Wiley, New York (1992).
- [14] X. Zong et. al., J. Am. Chem. Soc. **130**, 7176 (2008).
- [15] I.T. McGovern et. al., Surf. Sci. **152/153**, 1203 (1985).
- [16] B. Radisavljevic et. al., Nature Nanotechnology **6**, 147 (2011).
- [17] Y.B. Li, Y. Bando, and D. Golberg, Appl. Phys. Lett. **82**, 1962 (2003).
- [18] E. Gourmelon et. al., Sol. Energy Mater. Sol. Cells **46**, 115 (1997).
- [19] J. Chen et. al., J. Am. Chem. Soc. **123**, 11813 (2001).
- [20] J. Xiao et. al., Chem. Mater. **22**, 4522-4524 (2010).
- [21] K.F. Mak, C. Lee, J. Hone, J. Shan, and T.F. Heinz, Phys. Rev. Lett. **105**, 136805 (2010).
- [22] C. Lee et. al., ACS Nano **4**, 2695 (2011).
- [23] C. Ataca, M. Topsakal, E. Aktürk, and S. Ciraci, J. Phys. Chem. C **115**, 16354-16361 (2011).
- [24] H.H. Guo, T. Yang, P. Tao, Y. Wang, Z.D. Zhang, J. Appl. Phys. **113**, 013709 (2013).
- [25] C. Chiriac et. al., Science **315**, 351 (2007).
- [26] S.R. Guha Thakurta and A.K. Dutta, J. Phys. Chem. Solids **44**, 407 (1983).
- [27] R. Mansfield and S.A. Salam, Proc. Phys. Soc. B **66**, 377 (1953).
- [28] M.K. Agarwal and L.T. Talele, Sol. State Comm. **59**, 549 (1986).
- [29] J.-Y. Kim et. al., Bull. Korean Chem. Soc. **31**, 3225 (2010).
- [30] P. Blaha et. al., WIEN2k: An augmented plane wave plus local orbitals program for calculating crystal properties (TU Vienna, Vienna, 2011).
- [31] J.P. Perdew, K. Burke and M. Ernzerhof, Phys. Rev. Lett. **77**, 3865 (1996).
- [32] R. Coehoorn et. al., Phys. Rev. B **35**, 6195 (1987).
- [33] D. Parker, M.-H. Du, and D.J. Singh, Phys. Rev. B **83**, 245111 (2011).
- [34] L. Zhang and D.J. Singh, Phys. Rev. B **80**, 075117 (2009).
- [35] G.K.H. Madsen, K. Schwarz, P. Blaha, and D.J. Singh, Phys. Rev. B. **68**, 125212 (2003).
- [36] E. Engel and S.H. Vosko, Phys. Rev. B **47**, 13164 (1993).
- [37] S.W. Han et. al., Phys. Rev. B, **84**, 045409 (2011).
- [38] K.K. Kam and B.A. Parkinson, J. Phys. Chem. **86**, 463 (1982).
- [39] G.D. Mahan, "Good Thermoelectrics" in *Solid State Physics* vol. **51**, ed. by H. Ehrenreich and F. Seipen (Academic Press, San Diego, 1998).
- [40] D.M. Rowe and G. Min, J. Mater. Sci. Lett. **14**, 617-619 (1995).
- [41] Y. Zhang et al., Phys. Rev. Lett. **106**, 206601 (2011).
- [42] G.J. Snyder and E.S. Toberer, Nature Materials **7**, 105 (2008).
- [43] J. M. Ziman, *Principles of the theory of solids*, 2nd Ed.(Cambridge University Press, 1995)
- [44] K.P. Ong, D.J. Singh and P. Wu, Phys. Rev. Lett. **104**, 176601 (2010), K.P. Ong, J. Zhang, J.S. Tse and P. Wu, Phys. Rev. B **81**, 115120 (2010).
- [45] G.D. Tang, H.H. Guo, T. Yang and et. al., Appl. Phys. Lett. **98**, 202109 (2011).